The CPEB3 ribozyme modulates hippocampal-dependent memory

Authors

Claire C. Chen[1], Joseph Han[2], Carlene A. Chinn[2], Xiang Li[2†], Mehran Nikan[3], Marie Myszka[4], Liqi Tong[5], Timothy W. Bredy[2†], Marcelo A. Wood[2*], Andrej Lupták[1,4,6*]

Affiliations

[1] Department of Pharmaceutical Sciences, University of California–Irvine, Irvine, California 92697, United States.

[2] Department of Neurobiology and Behavior, Center for the Neurobiology of Learning and Memory, University of California–Irvine, Irvine, California 92697, United States.

[3] Ionis Pharmaceuticals, 2855 Gazelle Court, Carlsbad, CA 92010, USA.

[4] Department of Chemistry, University of California–Irvine, Irvine, California 92697, United States.

[5] Institute for Memory Impairments and Neurological Disorders, University of California–Irvine, Irvine, California 92697, United States.

[6] Department of Molecular Biology and Biochemistry, University of California–Irvine, Irvine, California 92697, United States

*Correspondence to: Andrej Lupták. Department of Pharmaceutical Sciences, University of California–Irvine, Irvine, California 92697, United States. aluptak@uci.edu. Marcelo A. Wood. Department of Neurobiology and Behavior, Center for the Neurobiology of Learning and Memory, University of California–Irvine, Irvine, California 92697, United States. mwood@uci.edu.

[†] Present address: Cognitive Neuroepigenetics Laboratory, Queensland Brain Institute, The University of Queensland, Brisbane, QLD 4072, Australia.

Abstract

A self-cleaving ribozyme mapping to an intron of the cytoplasmic polyadenylation element binding protein 3 (*CPEB3*) gene has been suggested to play a role in human episodic memory, but the underlying mechanisms mediating this effect are not known. The ribozyme's self-scission half-life matches the time it takes an RNA polymerase to reach the immediate downstream exon, suggesting that the ribozyme-dependent intron cleavage is tuned to co-transcriptional splicing of the *CPEB3* mRNA. Here we report that the murine ribozyme modulates its own host mRNA maturation in both cultured cortical neurons and the hippocampus. Inhibition of the ribozyme using an antisense oligonucleotide leads to increased CPEB3 protein expression, which enhances polyadenylation and translation of localized plasticity-related target mRNAs, and subsequently strengthens hippocampal-dependent long-term memory. These findings reveal a previously unknown role for self-cleaving ribozyme activity in regulating experience-induced co-transcriptional and local translational processes required for learning and memory.

Introduction

Self-cleaving ribozymes are catalytic RNAs that accelerate site-specific scission of their backbone [1]. Several mammalian ribozymes have been identified [2-9], including a functionally-conserved sequence that maps to the second intron of the cytoplasmic polyadenylation element binding protein (*CPEB3*) gene [4, 10, 11] (Fig 1A). The CPEB3 ribozyme shares its secondary structure and catalytic mechanism with the hepatitis delta virus (HDV) ribozymes [10, 12]. HDV-like ribozymes are widespread among genomes of eukaryotes [13-16] and their biological roles include processing of rolling-circle transcripts during HDV replication [2, 3], 5′-cleavage of retrotransposons [14-16], and in one bacterial example, potentially metabolite-dependent regulation of gene expression [17]. However, the

function of the mammalian ribozyme is unknown. In humans, a single nucleotide polymorphism (SNP) at the ribozyme cleavage site leads to a 3-fold higher rate of *in vitro* self-scission, which correlates with poorer performance in an episodic memory task [4, 18] and suggests that the ribozyme activity might play a role in memory formation.

CPEBs are RNA-binding proteins that modulate polyadenylation-induced mRNA translation, which is essential for the persistence of memory [19]. CPEBs have been found in several invertebrate and vertebrate genomes, and four *CPEB* genes (*CPEB1–4*) have been identified in mammals [20-24]. All CPEB proteins have two RNA recognition domains (RRM motifs) and a ZZ-type zinc finger domain in the C-terminal region, but differ in their N-terminal domains [25-27]. *Aplysia* CPEB (ApCPEB), *Drosophil*a Orb2, and mouse CPEB3 have two distinct functional conformations that correspond to soluble monomers and amyloidogenic oligomers, and have been implicated in maintenance of long-term facilitation (LTF) in *Aplysia* and long-term memory in both *Drosophil*a and mice [28-34]. In *Drosophil*a, inhibition of amyloid-like oligomerization of Orb2 impairs the persistence of long-lasting memory, and deletion of prion-like domain of Orb2 disrupts long-term courtship memory [32, 35]. The aggregated form of CPEB3, which is inhibited by SUMOylation, can mediate target mRNA translation at activated synapses [36].

Following synaptic stimulation CPEB3 interacts with actin cytoskeleton, with a positive feedback loop of CPEB3/actin regulating remodeling of synaptic structure and connections [37, 38]. Studies of CPEB3 in memory formation revealed that the local protein synthesis and long-term memory storage are regulated by the prion-like CPEB3 aggregates (the aggregation of CPEB3 is thought to strengthen synaptic plasticity in the hippocampus); *CPEB3* conditional knockout mice display impairments in memory consolidation, object

80 placement recognition, and long-term memory maintenance [31]. On the other hand, global
81 *CPEB3* knockout mice display enhanced spatial memory consolidation in the Morris water
82 maze and exhibit elevated short-term fear during the acquisition and extinction of contextual
83 fear memory [39].

84

85 The CPEB3 protein is thus well established as a modulator of memory formation and
86 learning, but the function of the CPEB3 ribozyme has not been tested. Given that the self-
87 scission of intronic ribozymes is inversely correlated with splicing efficiency of the harboring
88 pre-mRNA [40], we hypothesized that inhibition of the CPEB3 ribozyme co-transcriptional
89 self-self-cleavage can alter *CPEB3* mRNA splicing and increase the expression of full-length
90 mRNA and CPEB3 protein, leading to polyadenylation of its target mRNAs and an
91 enhancement in the consolidation of hippocampal-dependent memory.

92
93 ## Results
94

95 **CPEB3 mRNA expression and ribozyme activity are upregulated in response to**
96 **neuronal stimulation**

97 To test this hypothesis, we began by measuring the co-transcriptional self-scission of
98 the murine variant of the ribozyme *in vitro* and found a half-life ($t_{1/2}$) of ~2 minutes (Fig 1B
99 and Table S1), which is similar to previously measured chimp and fast-reacting human
100 variants of the ribozyme [41]. Because the distance from the ribozyme to the 3rd exon in the
101 *CPEB3* gene is about 10 kb and the RNA polymerase II (RNAPII) transcription rate of long
102 mammalian genes is estimated to be ~3.5–4.1 knt/min [42], RNAPII would take about 2.5–3

103 minutes to reach the 3rd exon and mark it for splicing. This result suggested that the ribozyme
104 activity is tuned to the co-transcriptional processing of the CPEB3 pre-mRNA.
105
106 The neuronal activity-dependent gene regulation is essential for synaptic plasticity
107 [43]. To investigate the effect of the CPEB3 ribozyme on *CPEB3* mRNA expression and
108 measure its effect on maturation and protein levels, we stimulated primary cortical neurons by
109 glutamate or potassium chloride (KCl). First, *CPEB3* mRNA levels were measured using
110 primers that specifically amplified exon–exon splice junctions (Exons 2–3, 3–6, 6–9; Fig 1A).
111 We found that membrane depolarization by KCl led to an up-regulation of *CPEB3* mRNA 2
112 hours post stimulation, compared with non-stimulated cultures (Fig 1C). To examine CPEB3
113 ribozyme activity, total ribozyme and uncleaved ribozyme levels were measured by qRT-
114 PCR, which showed that ribozyme expression is elevated at 1 hour following KCl treatment
115 (Fig 1D). Similarly, glutamate stimulation both increased the expression of spliced exons by
116 2–3 fold at 2 hours, with a decrease observed at later time points (Fig 1E), and increased
117 ribozyme expression correlated with CPEB3 mRNA expression (Fig 1F). This finding is
118 supported by previous studies showing that synaptic stimulation by glutamate leads to an
119 increase in CPEB3 protein expression in hippocampal neurons [31] and that treatment with
120 kainate likewise induces CPEB3 expression in the hippocampus [21]. The cleaved fraction of
121 the ribozyme was greatest at the highest point of CPEB3 mRNA expression, suggesting
122 efficient co-transcriptional self-scission. Together, these data (i) indicate that the self-cleaving
123 CPEB3 ribozyme is expressed, and potentially activated, in response to neuronal activity, and
124 (ii) suggest that CPEB3 ribozyme *cis*-regulates the maturation of CPEB3 mRNA.
125
126 **CPEB3 mRNA and protein levels increase in primary neuronal cultures treated with**
127 **ribozyme inhibitor**

128 Because our data showed that CPEB3 ribozyme expression is correlated with mRNA
129 expression, we hypothesized that regulation of the ribozyme may modulate CPEB3 mRNA
130 splicing. To test this hypothesis, we inhibited the ribozyme using antisense oligonucleotides
131 (ASOs) spanning the cleavage site (Figs 2A and 2B); these ASOs were similar to those
132 previously used to inhibit *in vitro* co-transcriptional self-scission of this family of ribozymes
133 [13, 44]. ASOs are synthetic single-stranded nucleic acids that can bind to pre-mRNA or
134 mature RNA through base-pairing, and typically trigger RNA degradation by RNase H,
135 thereby turning off the target gene expression. ASOs have also been used to modulate
136 alternative splicing, suggesting that they act co-transcriptionally (e.g., to correct the *SMN2*
137 mRNA) [45]. The ASOs used in this study were designed to increase thermal stability of
138 complementary hybridization and, as a result, to induce higher binding affinity for the
139 ribozyme.
140
141 To study the effect of the CPEB3 ribozyme on *CPEB3* mRNA expression, neuronal
142 cultures were pretreated with either an ASO or a non-targeting control oligonucleotide,
143 followed by KCl stimulation. In the absence of ASO, KCl induced a rapid and robust increase
144 in ribozyme levels compared to cultures containing scrambled ASO, and this effect was
145 suppressed in the presence of ASO, suggesting that the ribozyme is blocked by the ASO (S1A
146 Fig). At an early time point (2 hours post-KCl induction), the ASO-containing culture
147 displayed an increase of spliced mRNA (Figs 2C, S1 B and C), suggesting that the ASO
148 prevents CPEB3 ribozyme from cleaving the intron co-transcriptionally and promotes mRNA
149 maturation. At 24 hours post-KCl induction, we observed no significant difference in CPEB3
150 ribozyme expression among groups (S1D Fig). Likewise, the level of *CPEB3* mRNA exons
151 2–3 returned to the basal level (S1E Fig), while exons 3–6 remained slightly elevated in the
152 ASO-treatment groups (S1F Fig). The mRNA expression of CPEB3 exons 6–9 remained

153 stable over time and was not affected by ASO treatment or KCl stimulation (S1G Fig). Taken
154 together, these data suggest that the CPEB3 ribozyme modulates the production of the full-
155 length *CPEB3* mRNA.
156
157 To evaluate whether the ASO specifically targets CPEB3 ribozyme or modulates
158 intron levels in general, we measured the levels of the 4th CPEB3 intron, which does not
159 harbor a self-cleaving ribozyme. No significant difference in the 4th intron expression between
160 groups was observed, demonstrating that the ASO does not have a broad non-specific effect
161 on the stability of other introns (Fig S2H). Furthermore, to assess whether the ASO induces
162 cytotoxicity *in vitro*, neuronal cultures were treated with either ASO or scrambled ASO. Cell
163 viability was measured with an XTT assay, revealing no difference in either ASO- or
164 scrambled ASO-treated cells, compared to untreated cells. These data suggest that the ASOs
165 used in this study did not induce cytotoxic effects in cultured neurons (S1I Fig).
166
167 We next determined whether inhibition of CPEB3 ribozyme regulates CPEB3 protein
168 expression. Treatment with the ribozyme ASO resulted in a significant increase in CPEB3
169 protein levels in both the basal state and under KCl-stimulated conditions, indicating a
170 coordination of activity-dependent transcription and translation upon inhibition of CPEB3
171 ribozyme activity (Fig 2D).
172
173 **Ribozyme inhibition leads to increased expression of plasticity-related proteins**
174 In *Aplysia* sensory-motor neuron co-culture, application of repeated pulses of
175 serotonin (5-HT) induces ApCPEB protein expression at the stimulated synapses and LTF,
176 which is a form of learning-related synaptic plasticity that is widely studied in *Aplysia* [20,
177 29]. In murine primary hippocampal neurons, the level of CPEB3 protein expression is

178 positively regulated by neuronal activity [31] and plays dual roles in regulating mRNA
179 translation [37, 46] whereby a post-translational modification of CPEB3 can convert it from a
180 repressor to an activator: a monoubiquitination by Neuralized1 leads to activation of CPEB3,
181 which promotes subsequent polyadenylation and translation of GluA1 and GluA2 [47].
182 Previous studies have also demonstrated the role of CPEB3 in the translational regulation of a
183 number of plasticity-related proteins (PRPs), including AMPA-type glutamate receptors
184 (AMPARs), NMDA receptor (NMDAR), and postsynaptic density protein 95 (PSD-95) [26,
185 31, 39, 48]. As an RNA binding protein, CPEB3 has been shown to bind to 3′UTR of GluA1,
186 GluA2, and *PSD-95* mRNAs and to regulate their polyadenylation and translation [26, 31, 39,
187 47].
188
189 To test whether inhibition of CPEB3 ribozyme modulates expression of PRPs, we
190 measured the protein levels. We found that under KCl-induced depolarizing conditions,
191 treatment with the CPEB3 ribozyme ASO resulted in a significant increase in GluA1 and
192 PSD-95 protein expression, whereas GluA2 levels remained unchanged (S2A and S2B Fig).
193 Likewise, ASO treatment led to an up-regulation of NR2B protein, one of the NMDAR
194 subunits (S2C and S2D Fig). These results suggest that CPEB3 ribozyme activity affects
195 several downstream processes, particularly mRNA maturation and translation, as well as the
196 expression of PRPs, including the translation of AMPAR and NMDAR mRNAs.
197
198 **CPEB3 ribozyme ASO leads to an increase of CPEB3 mRNA and polyadenylation of**
199 **PRPs in the CA1 hippocampus**
200 To investigate whether the CPEB3 ribozyme exhibits similar effects in regulating
201 genes related to synaptic plasticity *in vivo*, mice were stereotaxically infused with either
202 ribozyme ASO, scrambled ASO, or vehicle into the CA1 region of the dorsal hippocampus, a

203 major brain region involved in memory consolidation and persistence (Fig 3A). Infusion of
204 ASO targeting the CPEB3 ribozyme significantly reduced ribozyme levels detected by RT-
205 qPCR in the dorsal hippocampus (S3A Fig). We found that administration of ASO led to an
206 increase of *CPEB3* mRNA in the CA1 hippocampus (Fig 3B), confirming that the ASO
207 prevents ribozyme self-scission during CPEB3 pre-mRNA transcription, thereby increasing
208 *CPEB3* mRNA levels. No significant difference in the ribozyme-free 4th intron levels was
209 observed between ASO and vehicle (S3B Fig).
210
211 Next, we tested whether the CPEB3 ribozyme inhibition affects CPEB3 translation,
212 and no significant difference between ASO and control groups was observed (S5A and S5B
213 Fig). We further observed that blocking the CPEB3 ribozyme does not change GluA1, GluA2,
214 PSD-95, and NR2B mRNA or protein expression in naïve mice (S4, S5A and S5C Fig). Thus,
215 in naïve mice, ribozyme inhibition leads to increased basal levels of the *CPEB3* mRNA, but
216 the levels of the CPEB3 protein and its downstream mRNA targets remain unchanged.
217
218 To further delineate whether the CPEB3 ribozyme activity results in polyadenylation
219 of its target mRNAs, 3′ rapid amplification of cDNA ends (3′ RACE) was performed to
220 examine the 3′ termini of several mRNAs. We found that ribozyme ASO administration led to
221 increased GluA1, GluA2, and PSD-95 mRNA polyadenylation in the mouse dorsal
222 hippocampus (Fig 3C). These data support a model wherein the inhibition of the CPEB3
223 ribozyme leads to increased polyadenylation of existing AMPARs and PSD-95 mRNAs, and
224 suggests a role in post-transcriptional regulation and 3′ mRNA processing.
225
226 **Inhibition of CPEB3 ribozyme in the dorsal hippocampus enhances long-term memory**

227 To assess whether inhibition of the CPEB3 ribozyme improves memory formation, we
228 tested it with respect to long-term memory using the object location memory (OLM) task (Fig
229 4A). The OLM task has been widely used to study hippocampal-dependent spatial memory.
230 The task is based on an animal's innate preference for novelty and its capability for
231 discriminating spatial relationships between novel and familiar locations [49]. During a
232 testing session, mice retrieve the memory that encoded for the objects they were exposed to in
233 the training session. We infused mice bilaterally into the CA1 dorsal hippocampus with the
234 CPEB3 ribozyme ASO, scrambled ASO, or vehicle 48 hours prior to OLM training. The
235 CPEB3 ribozyme ASO group showed a significant increase in discrimination index (DI)
236 between training and testing compared to control groups, suggesting that these mice
237 experienced a robust enhancement of novel object exploration (Fig 4B). We observed no
238 significant difference in training DI ($P > 0.05$), indicating that mice exhibit no preference for
239 either object (Fig 4B). Likewise, during training and testing sessions, ASO-infused mice and
240 control mice displayed similar total exploration time, demonstrating that both groups of mice
241 have similar exploitative behavior (Fig 4C). These results provide strong evidence that
242 CPEB3 is critical for long-term memory, and that the CPEB3 ribozyme activity is anti-
243 correlated with the formation of long-term memory.
244

245 **CPEB3 ribozyme ASO leads to an upregulation in protein expression of CPEB3 and**
246 **PRPs during memory consolidation**

247 Learning-induced changes in gene expression and protein synthesis are essential for
248 memory formation and consolidation [50]. To determine whether upregulation of CPEB3
249 mRNA by the ribozyme ASO leads to a change in expression of the CPEB3 protein and its
250 downstream targets, we analyzed the dorsal hippocampal homogenates and synaptosomal
251 fractions. Administration of CPEB3 ribozyme ASO led to a significant increase of CPEB3

252 protein expression in the CA1 hippocampal homogenates and crude synaptosomes 1 hour
253 after OLM testing (Figs 5, A, B, and D). This result confirms that ASO-mediated knockdown
254 of the CPEB3 ribozyme facilitates CPEB3 mRNA processing and translation. The protein
255 levels of GluA1, GluA2, PSD-95, and NR2B were measured to determine whether increased
256 CPEB3 further regulates translation of PRPs. In total tissue lysates, no significant difference
257 in PRPs levels was observed between ASO and control (Figs 5, A and C). However, in
258 synaptosomal fractions, GluA1, PSD-95, and NR2B protein levels were increased in ASO-
259 infused mice, relative to scrambled ASO control animals; and GluA2 protein level remained
260 unaffected (Figs 5, A and E). Our findings thus show that blocking CPEB3 ribozyme activity
261 leads to an increase in CPEB3 protein production, and up-regulation of CPEB3 by OLM
262 further mediates local GluA1, PSD-95, and NR2B translation.

263
264
265 **Discussion**
266
267 Self-cleaving ribozymes are broadly distributed small functional RNAs that catalyze a
268 site-specific scission of their backbone [1]. The HDV family of these ribozymes acts during
269 rolling circle replication of the HDV RNA genome and in processing of retrotransposons [2,
270 3, 14-16], but given their broad distribution in nature, their biological roles are largely
271 unexplored. Mammals harbor several self-cleaving ribozymes—all without known biological
272 functions [4-9]. One of these ribozymes, the HDV-like CPEB3 ribozyme, maps to the second
273 intron of the *CPEB3* gene and its *in vitro* activity (Figs 1A and 1B) suggested that its rate of
274 self-scission may be tuned to disrupt the intron at a rate that is similar to the production speed
275 of the downstream intronic sequence ahead of the next exon. Previous work on synthetic
276 ribozymes placed within introns of mammalian genes showed that splicing of the surrounding
277 exons is sensitive to the continuity of the intron: fast ribozymes caused efficient self-scission
278 of the intron, leading to unspliced mRNA and resulting in lower protein expression, whereas

279 slow ribozymes had no effect on mRNA splicing and subsequent protein expression [40].
280 Inspired by this work, we investigated how the intronic ribozyme affects the *CPEB3* mRNA
281 maturation and translation, and its effect on memory formation in mice.
282
283 Modifications of synaptic strength are thought to underlie learning and memory in the
284 brain. Studies in hippocampal slices revealed local translation in dendrites following
285 induction of LTP [51]. Cytoplasmic polyadenylation-induced translation is one of the key
286 steps for regulating protein synthesis and neuroplasticity [22, 46, 52]. One of the proteins
287 involved in regulation of cytoplasmic polyadenylation of mRNAs is CPEB3. Recent studies
288 have shown that CPEB3 regulates mRNA translation of several PRPs at synapses, where it is
289 essential for synaptic strength [26, 31, 47]. Previous reports have shown that CPEB3 regulates
290 GluA1 and GluA2 polyadenylation: CPEB3 conditional knockout mice fail to elongate the
291 poly(A) tail of GluA1 and GluA2 mRNA after Morris water maze training, and
292 overexpression of CPEB3 changes the length of the GluA1 and GluA2 mRNA poly(A) tail
293 [31]. Even though translational control by regulation of CPEB3 has been demonstrated to
294 contribute to the hippocampal-dependent learning and memory [47], one unaddressed
295 question is whether the CPEB3 expression is modulated by the CPEB3 ribozyme. In
296 mammals, the coordination of pre-mRNA processing and transcription can affect its gene
297 expression [53]. Recent measurement of co-transcriptional splicing events in mammalian cells
298 using long-read sequencing and Precision Run-On sequencing (PRO-seq) approaches
299 demonstrated that co-transcriptional splicing efficiency impacts productive gene output [54].
300 The temporal and spatial window shows that the splicing and transcription machinery are
301 tightly coupled. In agreement with this co-transcriptional splicing model, our study shows that
302 inhibition of the intronic CPEB3 ribozyme leads to an increase in *CPEB3* mRNA and protein

303 levels in primary cortical neurons and the dorsal hippocampus upon synaptic stimulation, and
304 leading to changes in polyadenylation of target mRNAs of the CPEB3 protein.
305
306 Activity-dependent synaptic changes are governed by AMPAR trafficking, and
307 AMPARs are mobilized to the post-synaptic surface membrane in response to neuronal
308 activity in a dynamic process [55]. Our data demonstrate that the activation of CPEB3 by
309 neuronal stimulation further facilitates translation of PRPs *in vivo*. These observations are
310 consistent with a model in which learning induces CPEB3 protein expression, and ablation of
311 CPEB3 abolishes the activity-dependent translation of GluA1 and GluA2 in the mouse
312 hippocampus [31]. Specifically, it has been suggested that CPEB3 converts to prion-like
313 aggregates in stimulated synapses that mediate hippocampal synaptic plasticity and facilitate
314 memory storage [56]. Because training can produce effective long-term memory, it is likely
315 that increased CPEB3 protein expression due CPEB3 ribozyme inhibition further facilitates
316 experience-induced local translational processes.
317
318 ASOs have been used in many studies to inhibit specific mRNAs. A notable example
319 is an FDA-approved ASO that modulates co-transcriptional splicing of the *SMN2* mRNA
320 [45]. Our works shows that an ASO designed to bind the substrate strand of an endogenous
321 self-cleaving ribozyme located in an intron increases the expression of the fully spliced
322 mRNA that harbors the ribozyme. Interestingly, experiments with inhibitory ASO yielded
323 lower the ribozyme levels than control experiments, suggesting that the ASO directs
324 degradation of the target sequence; however, this degradation must occur on a timescale that
325 is longer than the splicing of the mRNA, because we consistently see higher mRNA levels
326 when the ribozyme is inhibited. Further studies will be necessary to delineate the full
327 mechanism of action of anti-ribozyme ASOs. Given that three endogenous mammalian self-

328 cleaving ribozymes map to introns [4, 6, 7], we anticipate that application of ASOs will help
329 decipher their effect on their harboring mRNAs and establish their biological roles.
330
331 In summary, we have delineated an important step in molecular mechanisms
332 underlying a unique role for the CPEB3 ribozyme in post-transcriptional maturation of
333 CPEB3 mRNA and its subsequent translation in mouse CA1 hippocampus. Inhibition of the
334 CPEB3 ribozyme by ASO and OLM training induce activity-dependent upregulation of
335 CPEB3 and local production of PRPs. These molecular changes are critical for establishing
336 persistent changes in synaptic plasticity that are required for long-term memory, and represent
337 a biological role for self-cleaving ribozymes in the brain. More broadly, our study
338 demonstrates a novel biological role for self-cleaving ribozymes and the first example of their
339 function in mammals.
340
341
342 ## Materials and Methods
343
344 **Primary cortical neuronal culture**
345 Pregnant female C57BL/6 mice (The Jackson Laboratory) were euthanized at E18,
346 and embryos were collected into an ice-cold Neurobasal medium (Thermo Fisher Scientific).
347 Embryonic cortices were dissected, meninges were removed, and tissues were minced. Cells
348 were mechanically dissociated, passed through a 40-µm cell strainer, counted, and plated at a
349 density of 0.5 x 10^6 cells per well in six-well plates coated with poly-D-lysine (Sigma-
350 Aldrich). Neuronal cultures were maintained at 37 °C with 5% CO_2, and grown in Neurobasal
351 medium containing 2% B27 supplement (Thermo Fisher Scientific), 1%
352 penicillin/streptomycin (Thermo Fisher Scientific), and 2 mM L-Glutamine (Thermo Fisher
353 Scientific) for 7–10 days *in vitro* (DIV), with 50% of the medium being replaced every 3
354 days. All experimental procedures were performed according to the National Institutes of

355 Health Guide for the Care and Use of Laboratory Animals and approved by the Institutional
356 Animal Care and Use Committee of the University of California, Irvine.
357
358 **Mice**
359 C57BL/6J mice (8–10 weeks old, The Jackson Laboratory) were housed in a 12-h
360 light/dark cycle and had free access to water and food. All experiments were conducted
361 during the light cycle. All experimental procedures were performed according to the National
362 Institutes of Health Guide for the Care and Use of Laboratory Animals and approved by the
363 Institutional Animal Care and Use Committee of the University of California, Irvine.
364
365 **Measurement of co-transcriptional self-scission of the CPEB3 ribozyme**
366 Transcription reactions were set up in a 5-μL volume and incubated for 10 minutes at
367 25 ºC, as described previously [17]. The reactions contained: 1 μL of 5x transcription buffer
368 (10 mM spermidine, 50 mM dithiothreitol, 120 mM Tris chloride buffer, pH 7.5, and 0.05%
369 Triton X-100), 1 μL of 5x ribonucleoside triphosphates (final concentration of 6.8 mM), 1 μL
370 of 5 mM Mg^{2+}, 1 μL DNA amplified by PCR to about 1 μM final concentration, 0.5 μL of
371 100% DMSO, 0.15 μL of water, 0.1 μL of murine RNase inhibitor (40,000 units/mL, New
372 England Biolabs), 0.125 μL of T7 polymerase, and 0.125 μL [α-^{32}P]ATP. To prevent
373 initiation of new transcription, the reactions were diluted into 100 μL of physiological-like
374 buffer solution at 37 ºC. The solution consisted of 2 mM Mg^{2+} (to promote ribozyme self-
375 scission), 140 mM KCl, 10 mM NaCl, and 50 mM Tris chloride buffer (pH 7.5). The 100-μL
376 solution was then held at 37 ºC for the reminder of the experiment while aliquots were
377 withdrawn at various time points. An equal volume of 4 mM EDTA/7 M urea stopping
378 solution was added to each aliquot collected. Aliquots were resolved using denaturing
379 polyacrylamide gel electrophoresis (PAGE, 7.5% polyacrylamide, 7 M urea) at 20 W. The

380 PAGE gel was exposed to a phosphosimage screen for ~2 hours and analyzed using a
381 Amersham Typhoon imaging system (GE Healthcare). Band intensities corresponding to the
382 uncleaved ribozymes and the two products of self-scission were analyzed using ImageQuant
383 (GE Healthcare) and exported into Excel. Fraction Intact was calculated as the intensity of the
384 band corresponding to the uncleaved ribozyme divided by the sum of band intensities in a
385 given PAGE lane. The data were fit to a biexponential decay model:

386 $k_{\text{obs}} = \text{A} \times \text{e}^{-k(1)t} + \text{B} \times \text{e}^{-k(2)t} + C$

387 In the case of the minimum murine CPEB3 ribozyme construct (-10/72; S2 Fig and
388 Table S1), the data were modeled by a monoexponential decay with an uncleaved fraction
389 (using parameters A, k_1, and C only).

390

391 **Antisense oligonucleotides (ASOs)**

392 ASOs used in this study are 20 nucleotides in length and are chemically modified with
393 2′-*O*-methoxyethyl (MOE, underlined) and 2′-4′ constrained ethyl (cEt, bold) [57]. All
394 internucleoside linkages are modified with phosphorothioate linkages to improve nuclease
395 resistance. ASOs were solubilized in sterile phosphate-buffered saline (PBS). The sequences
396 of the ASOs are as follows (all cytosine nucleobases are 5-methyl substituted):

397 Scrambled control ASO: 5′-C<u>CT</u>T<u>CC</u>C<u>TG</u>A<u>AG</u>G<u>TT</u>C<u>CT</u>C<u>C</u>-3′;

398 CPEB3 ribozyme ASO: 5′-T<u>GT</u>G<u>GC</u>C<u>CC</u>C<u>TG</u>T<u>TA</u>T<u>CC</u>T<u>C</u>-3′.

399

400 **Neuronal stimulation**

401 Neurons were treated with ASO or scrambled ASO (1 μM) for 18 hours prior to
402 neuronal stimulation. To study activity-dependent gene regulation, neuronal cultures were
403 treated with vehicle, 5 μM glutamate (10 minutes), or 35 mM KCl (5 minutes). After

404 stimulation, cultures were washed with Hanks' buffered salt solution (HBSS, Thermo Fisher
405 Scientific), and then replaced with fresh medium.

406

407 **Quantitative RT-PCR analysis**

408 Total RNA was isolated from primary cortical neurons or mouse hippocampus using
409 TRI reagent (Sigma-Aldrich) according to the manufacturer's protocol. RNA concentration
410 was measured using a NanoDrop ND-1000 spectrophotometer (Thermo Fisher Scientific).
411 Total RNA was reverse transcribed using random decamers and M-MLV reverse transcriptase
412 (Promega)/Superscript II RNase H reverse transcriptase (Thermo Fisher Scientific).
413 Quantitative RT-PCR was performed on a BioRad CFX Connect system using iTaq Universal
414 SYBR Green Supermix (BioRad). Designed primers were acquired from Integrated DNA
415 Technologies and provided in Table S2. Desired amplicons were verified by melting curve
416 analysis and followed by gel electrophoresis. The starting quantity of DNA from each sample
417 was determined by interpolation of the threshold cycle (CT) from a standard curve of each
418 primer set. Relative gene expression levels were normalized to the endogenous gene *GAPDH*.

419

420 **Immunoblotting**

421 Primary cortical neurons or mouse hippocampal tissues were lysed in RIPA lysis
422 buffer with protease inhibitor (Santa Cruz Biotechnology). Crude synaptosomal fractions
423 were prepared as previously described [58]. Protein concentrations were measured using
424 bicinchoninic acid (BCA) protein assay (Thermo Fisher Scientific). Ten to 30 μg of protein
425 samples were loaded on 10% sodium dodecyl sulfate polyacrylamide (SDS-PAGE) gels and
426 separated by electrophoresis. Gels were electro-transferred onto polyvinylidene fluoride
427 (PVDF) membranes using a semi-dry transfer system (BioRad). Membranes were either

428 blocked with 5% nonfat milk or 5% bovine serum albumin (BSA) in Tris-buffered
429 saline/Tween 20 (0.1% [vol/vol]) (TBST) for 1 hour at room temperature. Membranes were
430 incubated with primary antibodies overnight at 4 ºC. After primary antibody incubation,
431 membranes were washed three times with TBST and then incubated with secondary
432 antibodies for 1 hour at room temperature. Bands were detected using an enhanced
433 chemiluminescence (ECL) kit (Thermo Fisher Scientific), visualized using BioRad Chemidoc
434 MP imaging system, and analyzed by Image Lab software (BioRad). GAPDH was used as a
435 loading control. All antibodies used in this study are listed in Table S3.

436

437 ***In vitro* XTT cell viability assay**

438 Primary cortical neurons (10,000 to 20,000 cells/well) were plated onto 96-well plates
439 coated with poly-D-lysine. After 7–14 days, ASOs or scrambled ASOs were added and
440 incubated for 18 hours. Cell viability was determined using the 2,3-bis[2-methoxy-4-nitro-5-
441 sulfophenyl]-2H-tetrazolium-5-carboxyanilide inner salt (XTT) assay according to the
442 manufacturer's protocol (Biotium). The assay utilizes the ability of viable cells with active
443 metabolism to reduce the yellow tetrazolium salt to the soluble orange formazan product by
444 mitochondrial dehydrogenase enzymes. The XTT reagent was added to each well and
445 incubated for 2–4 hours at 37 °C and 5% CO_2. Absorbance was measured at 450 nm with a
446 reference wavelength of 680 nm using a Biotek Synergy HT microplate reader. Results were
447 normalized to control, and all samples were assayed in triplicate.

448

449 **Stereotaxic surgeries**

450 C57/BL6J mice (8–10 weeks old, Jackson Laboratory), housed under standard
451 conditions with light-control (12-h light/12-h dark cycles), were anaesthetized with an
452 isoflurane (1–3%)/oxygen vapor mixture. Mice were infused bilaterally to the CA1 region of

453 the dorsal hippocampus with ribozyme ASO, scrambled ASO diluted in sterile PBS, or
454 vehicle. The following coordinates were used, relative to bregma: medial-lateral (ML), ±1.5
455 mm; anterior-posterior (AP), −2.0 mm; dorsal-ventral (DV), −1.5 mm. ASOs or vehicle (1
456 nmol/μL) were infused bilaterally at a rate of 0.1 μL/min using a Neuros Hamilton syringe
457 (Hamilton company) with a syringe pump (Harvard Apparatus). The injectors were left in
458 place for 2 minutes to allow diffusion, and then were slowly removed at a rate of 0.1 mm per
459 15 sec. The incision site was sutured, and mice were allowed to recover on a warming pad and
460 then were returned to cages. For all surgeries, mice were randomly assigned to the different
461 conditions to avoid grouping same treatment conditions in time.

462

463 **Object location memory (OLM) tasks**

464 The OLM was performed to assess hippocampus-dependent memory, as previously
465 described [49]. Briefly, naïve C57/BL6J mice (8–12 weeks old; n = 10–12/group; ribozyme
466 ASO, scrambled ASO) were trained and tested. Prior to training, mice were handled 1–2
467 minutes for 5 days and then habituated to the experimental apparatus for 5 minutes on 6
468 consecutive days in the absence of objects. During training, mice were placed into the
469 apparatus with two identical objects and allowed to explore the objects for 10 minutes.
470 Twenty-four hours after training, mice were exposed to the same arena, and long-term
471 memory was tested for 5 minutes, with the two identical objects present, one of which was
472 placed in a novel location. For all experiments, objects and locations were counterbalanced
473 across all groups to reduce bias. Videos of training and testing sessions were analyzed for
474 discrimination index (DI) and total exploration time of objects. The videos were scored by
475 observers blind to the treatment. The exploration of the objects was scored when the mouse's
476 snout was oriented toward the object within a distance of 1 cm or when the nose was touching
477 the object. The relative exploration time was calculated as a discrimination index (DI = (t_{novel}

478 $- t_{familiar}) / (t_{novel} + t_{familiar}) \times 100\%$). Mice that demonstrated a location or an object preference
479 during the training trial (DI > ±20) were removed from analysis.

480

481 **3′ RACE**

482 Total RNA was extracted from the mouse CA1 hippocampus. 3′ rapid amplification of
483 cDNA ends (3′ RACE) was performed to study the alternative polyadenylation. cDNA was
484 synthesized using oligo(dT) primers with 3′ RACE adapter primer sequence at the 5′ ends.
485 This cDNA library results in a universal sequence at the 3′ end. A gene-specific primer (GSP)
486 and an anchor primer that targets the poly(A) tail region were used for the first PCR using the
487 following protocol: 95 °C for 3 minutes, followed by 30 cycles of 95 °C for 30 seconds, 55 °C
488 for 30 seconds, and 72 °C for 3 minutes, with a final extension of 72 °C for 5 minutes. To
489 improve specificity, a nested PCR was then carried out using primers internal to the first two
490 primers. Upon amplification condition optimization, a quantitative PCR was performed on the
491 first diluted PCR product using the nested primers, and a standard curve of the primer set was
492 generated to determine the effect of relative expression of 3′-mRNA and alternative
493 polyadenylation. All primers used in this study are listed in Table S4. When resolved using
494 agarose gel electrophoresis, this nested-primer qPCR produced single bands corresponding to
495 the correct amplicons of individual cDNAs.

496

497 **Statistical analysis**

498 Data are presented as means ± SEM. Statistical analyses were performed using
499 GraphPad Prism (GraphPad Prism Software). Statistical differences were determined using
500 two-tailed Welch's *t* test when comparing between 2 independent groups, and one-way
501 ANOVA with Sidak's *post hoc* tests when comparing across 3 or more independent groups.

502 OLM data were analyzed with two-way ANOVA followed by Sidak's *post hoc* tests. $P < 0.05$

503 was considered significant.

504
505
506

507 # References
508

509 1. Jimenez RM, Polanco JA, Luptak A. Chemistry and Biology of Self-Cleaving Ribozymes.
510 Trends Biochem Sci. 2015;40(11):648-61. doi: 10.1016/j.tibs.2015.09.001. PubMed PMID:
511 26481500; PubMed Central PMCID: PMCPMC4630146.
512 2. Sharmeen L, Kuo MY, Dinter-Gottlieb G, Taylor J. Antigenomic RNA of human hepatitis delta
513 virus can undergo self-cleavage. J Virol. 1988;62(8):2674-9. PubMed PMID: 2455816; PubMed
514 Central PMCID: PMCPMC253699.
515 3. Wu HN, Lin YJ, Lin FP, Makino S, Chang MF, Lai MMC. Human Hepatitis-Delta Virus-Rna
516 Subfragments Contain an Autocleavage Activity. P Natl Acad Sci USA. 1989;86(6):1831-5. doi:
517 DOI 10.1073/pnas.86.6.1831. PubMed PMID: WOS:A1989T788900019.
518 4. Salehi-Ashtiani K, Luptak A, Litovchick A, Szostak JW. A genomewide search for ribozymes
519 reveals an HDV-like sequence in the human CPEB3 gene. Science. 2006;313(5794):1788-92.
520 doi: 10.1126/science.1129308. PubMed PMID: 16990549.
521 5. Martick M, Horan LH, Noller HF, Scott WG. A discontinuous hammerhead ribozyme embedded
522 in a mammalian messenger RNA. Nature. 2008;454(7206):899-U57. doi: 10.1038/nature07117.
523 PubMed PMID: WOS:000258398600039.
524 6. de la Pena M, Garcia-Robles I. Intronic hammerhead ribozymes are ultraconserved in the human
525 genome. Embo Rep. 2010;11(9):711-6. doi: 10.1038/embor.2010.100. PubMed PMID:
526 WOS:000281467200016.
527 7. Perreault J, Weinberg Z, Roth A, Popescu O, Chartrand P, Ferbeyre G, et al. Identification of
528 Hammerhead Ribozymes in All Domains of Life Reveals Novel Structural Variations. Plos
529 Comput Biol. 2011;7(5). doi: ARTN e1002031
530 10.1371/journal.pcbi.1002031. PubMed PMID: WOS:000291015800014.
531 8. Chen Y, Qi F, Gao F, Cao HF, Xu DY, Salehi-Ashtiani K, et al. Hovlinc is a recently evolved
532 class of ribozyme found in human lncRNA. Nat Chem Biol. 2021. doi: 10.1038/s41589-021-
533 00763-0. PubMed PMID: WOS:000631491100002.
534 9. Hernandez AJ, Zovoilis A, Cifuentes-Rojas C, Han L, Bujisic B, Lee JT. B2 and ALU
535 retrotransposons are self-cleaving ribozymes whose activity is enhanced by EZH2. P Natl Acad
536 Sci USA. 2020;117(1):415-25. doi: 10.1073/pnas.1917190117. PubMed PMID:
537 WOS:000506001200062.
538 10. Webb CH, Luptak A. HDV-like self-cleaving ribozymes. RNA Biol. 2011;8(5):719-27. doi:
539 10.4161/rna.8.5.16226. PubMed PMID: 21734469; PubMed Central PMCID:
540 PMCPMC3256349.
541 11. Bendixsen DP, Pollock TB, Peri G, Hayden EJ. Experimental Resurrection of Ancestral
542 Mammalian CPEB3 Ribozymes Reveals Deep Functional Conservation. Molecular Biology and
543 Evolution. 2021. doi: 10.1093/molbev/msab074.
544 12. Skilandat M, Rowinska-Zyrek M, Sigel RK. Secondary structure confirmation and localization
545 of Mg2+ ions in the mammalian CPEB3 ribozyme. RNA. 2016;22(5):750-63. doi:
546 10.1261/rna.053843.115. PubMed PMID: 26966151; PubMed Central PMCID:
547 PMCPMC4836649.
548 13. Webb CH, Riccitelli NJ, Ruminski DJ, Luptak A. Widespread occurrence of self-cleaving
549 ribozymes. Science. 2009;326(5955):953. doi: 10.1126/science.1178084. PubMed PMID:
550 19965505; PubMed Central PMCID: PMCPMC3159031.
551 14. Ruminski DJ, Webb CH, Riccitelli NJ, Luptak A. Processing and translation initiation of non-
552 long terminal repeat retrotransposons by hepatitis delta virus (HDV)-like self-cleaving
553 ribozymes. J Biol Chem. 2011;286(48):41286-95. doi: 10.1074/jbc.M111.297283. PubMed
554 PMID: 21994949; PubMed Central PMCID: PMCPMC3308841.

555 15. Eickbush DG, Eickbush TH. R2 Retrotransposons Encode a Self-Cleaving Ribozyme for
556 Processing from an rRNA Cotranscript. Molecular and Cellular Biology. 2010;30(13):3142-50.
557 doi: 10.1128/Mcb.00300-10. PubMed PMID: WOS:000278626100001.
558 16. Sanchez-Luque FJ, Lopez MC, Macias F, Alonso C, Thomas MC. Identification of an hepatitis
559 delta virus-like ribozyme at the mRNA 5 '-end of the L1Tc retrotransposon from Trypanosoma
560 cruzi. Nucleic Acids Research. 2011;39(18):8065-77. doi: 10.1093/nar/gkr478. PubMed PMID:
561 WOS:000295687700023.
562 17. Passalacqua LFM, Jimenez RM, Fong JY, Luptak A. Allosteric Modulation of the
563 Faecalibacterium prausnitzii Hepatitis Delta Virus-like Ribozyme by Glucosamine 6-Phosphate:
564 The Substrate of the Adjacent Gene Product. Biochemistry-Us. 2017;56(45):6006-14. doi:
565 10.1021/acs.biochem.7b00879. PubMed PMID: 29045794; PubMed Central PMCID:
566 PMCPMC5775185.
567 18. Vogler C, Spalek K, Aerni A, Demougin P, Muller A, Huynh KD, et al. CPEB3 is associated
568 with human episodic memory. Front Behav Neurosci. 2009;3:4. doi: 10.3389/neuro.08.004.2009.
569 PubMed PMID: 19503753; PubMed Central PMCID: PMCPMC2691156.
570 19. Huang YS, Carson JH, Barbarese E, Richter JD. Facilitation of dendritic mRNA transport by
571 CPEB. Genes Dev. 2003;17(5):638-53. doi: 10.1101/gad.1053003. PubMed PMID: 12629046;
572 PubMed Central PMCID: PMCPMC196011.
573 20. Si K, Giustetto M, Etkin A, Hsu R, Janisiewicz AM, Miniaci MC, et al. A neuronal isoform of
574 CPEB regulates local protein synthesis and stabilizes synapse-specific long-term facilitation in
575 aplysia. Cell. 2003;115(7):893-904. doi: 10.1016/s0092-8674(03)01021-3. PubMed PMID:
576 14697206.
577 21. Theis M, Si K, Kandel ER. Two previously undescribed members of the mouse CPEB family of
578 genes and their inducible expression in the principal cell layers of the hippocampus. Proc Natl
579 Acad Sci U S A. 2003;100(16):9602-7. doi: 10.1073/pnas.1133424100. PubMed PMID:
580 12871996; PubMed Central PMCID: PMCPMC170964.
581 22. Richter JD. CPEB: a life in translation. Trends Biochem Sci. 2007;32(6):279-85. doi:
582 10.1016/j.tibs.2007.04.004. PubMed PMID: 17481902.
583 23. Afroz T, Skrisovska L, Belloc E, Guillen-Boixet J, Mendez R, Allain FHT. A fly trap
584 mechanism provides sequence-specific RNA recognition by CPEB proteins. Gene Dev.
585 2014;28(13):1498-514. doi: 10.1101/gad.241133.114. PubMed PMID: WOS:000338816000010.
586 24. Merkel DJ, Wells SB, Hilburn BC, Elazzouzi F, Alvarado GCP, Lee BM. The C-Terminal
587 Region of Cytoplasmic Polyadenylation Element Binding Protein Is a ZZ Domain with Potential
588 for Protein-Protein Interactions. Journal of Molecular Biology. 2013;425(11):2015-26. doi:
589 10.1016/j.jmb.2013.03.009. PubMed PMID: WOS:000320419300012.
590 25. Hake LE, Richter JD. CPEB is a specificity factor that mediates cytoplasmic polyadenylation
591 during Xenopus oocyte maturation. Cell. 1994;79(4):617-27. PubMed PMID: 7954828.
592 26. Huang YS, Kan MC, Lin CL, Richter JD. CPEB3 and CPEB4 in neurons: analysis of RNA-
593 binding specificity and translational control of AMPA receptor GluR2 mRNA. Embo J.
594 2006;25(20):4865-76. doi: 10.1038/sj.emboj.7601322. PubMed PMID: 17024188; PubMed
595 Central PMCID: PMCPMC1618119.
596 27. Ivshina M, Lasko P, Richter JD. Cytoplasmic polyadenylation element binding proteins in
597 development, health, and disease. Annu Rev Cell Dev Biol. 2014;30:393-415. doi:
598 10.1146/annurev-cellbio-101011-155831. PubMed PMID: 25068488.
599 28. Miniaci MC, Kim JH, Puthanveettil SV, Si K, Zhu H, Kandel ER, et al. Sustained CPEB-
600 dependent local protein synthesis is required to stabilize synaptic growth for persistence of long-
601 term facilitation in Aplysia. Neuron. 2008;59(6):1024-36. doi: 10.1016/j.neuron.2008.07.036.
602 PubMed PMID: 18817739; PubMed Central PMCID: PMCPMC3442368.

603 29. Si K, Choi YB, White-Grindley E, Majumdar A, Kandel ER. Aplysia CPEB can form prion-like
604 multimers in sensory neurons that contribute to long-term facilitation. Cell. 2010;140(3):421-35.
605 doi: 10.1016/j.cell.2010.01.008. PubMed PMID: 20144764.
606 30. Majumdar A, Cesario WC, White-Grindley E, Jiang H, Ren F, Khan MR, et al. Critical role of
607 amyloid-like oligomers of Drosophila Orb2 in the persistence of memory. Cell.
608 2012;148(3):515-29. doi: 10.1016/j.cell.2012.01.004. PubMed PMID: 22284910.
609 31. Fioriti L, Myers C, Huang YY, Li X, Stephan JS, Trifilieff P, et al. The Persistence of
610 Hippocampal-Based Memory Requires Protein Synthesis Mediated by the Prion-like Protein
611 CPEB3. Neuron. 2015;86(6):1433-48. doi: 10.1016/j.neuron.2015.05.021. PubMed PMID:
612 26074003.
613 32. Hervas R, Li LY, Majumdar A, Fernandez-Ramirez MD, Unruh JR, Slaughter BD, et al.
614 Molecular Basis of Orb2 Amyloidogenesis and Blockade of Memory Consolidation. Plos
615 Biology. 2016;14(1). doi: ARTN e1002361
616 10.1371/journal.pbio.1002361. PubMed PMID: WOS:000371882900026.
617 33. Rayman JB, Kandel ER. Functional Prions in the Brain. Cold Spring Harb Perspect Biol.
618 2017;9(1). doi: 10.1101/cshperspect.a023671. PubMed PMID: 28049644; PubMed Central
619 PMCID: PMCPMC5204323.
620 34. Hervas R, Rau MJ, Park Y, Zhang W, Murzin AG, Fitzpatrick JAJ, et al. Cryo-EM structure of a
621 neuronal functional amyloid implicated in memory persistence in Drosophila. Science.
622 2020;367(6483):1230-4. doi: 10.1126/science.aba3526. PubMed PMID: 32165583; PubMed
623 Central PMCID: PMCPMC7182444.
624 35. Keleman K, Kruttner S, Alenius M, Dickson BJ. Function of the Drosophila CPEB protein Orb2
625 in long-term courtship memory. Nat Neurosci. 2007;10(12):1587-93. doi: 10.1038/nn1996.
626 PubMed PMID: 17965711.
627 36. Drisaldi B, Colnaghi L, Fioriti L, Rao N, Myers C, Snyder AM, et al. SUMOylation Is an
628 Inhibitory Constraint that Regulates the Prion-like Aggregation and Activity of CPEB3. Cell
629 Rep. 2015;11(11):1694-702. doi: 10.1016/j.celrep.2015.04.061. PubMed PMID: 26074071.
630 37. Stephan JS, Fioriti L, Lamba N, Colnaghi L, Karl K, Derkatch IL, et al. The CPEB3 Protein Is a
631 Functional Prion that Interacts with the Actin Cytoskeleton. Cell Rep. 2015;11(11):1772-85. doi:
632 10.1016/j.celrep.2015.04.060. PubMed PMID: 26074072.
633 38. Gu XY, Schafer NP, Wang Q, Song SS, Chen MC, Waxham MN, et al. Exploring the F-
634 actin/CPEB3 interaction and its possible role in the molecular mechanism of long-term memory.
635 P Natl Acad Sci USA. 2020;117(36):22128-34. doi: 10.1073/pnas.2012964117. PubMed PMID:
636 WOS:000572964500015.
637 39. Chao HW, Tsai LY, Lu YL, Lin PY, Huang WH, Chou HJ, et al. Deletion of CPEB3 enhances
638 hippocampus-dependent memory via increasing expressions of PSD95 and NMDA receptors. J
639 Neurosci. 2013;33(43):17008-22. doi: 10.1523/JNEUROSCI.3043-13.2013. PubMed PMID:
640 24155305.
641 40. Fong N, Ohman M, Bentley DL. Fast ribozyme cleavage releases transcripts from RNA
642 polymerase II and aborts co-transcriptional pre-mRNA processing. Nat Struct Mol Biol.
643 2009;16(9):916-22. doi: 10.1038/nsmb.1652. PubMed PMID: 19701200; PubMed Central
644 PMCID: PMCPMC2755206.
645 41. Chadalavada DM, Gratton EA, Bevilacqua PC. The human HDV-like CPEB3 ribozyme is
646 intrinsically fast-reacting. Biochemistry-Us. 2010;49(25):5321-30. doi: 10.1021/bi100434c.
647 PubMed PMID: 20524672; PubMed Central PMCID: PMCPMC2890282.
648 42. Singh J, Padgett RA. Rates of in situ transcription and splicing in large human genes. Nat Struct
649 Mol Biol. 2009;16(11):1128-33. doi: 10.1038/nsmb.1666. PubMed PMID: 19820712; PubMed
650 Central PMCID: PMCPMC2783620.

651 43. Neves G, Cooke SF, Bliss TV. Synaptic plasticity, memory and the hippocampus: a neural
652 network approach to causality. Nat Rev Neurosci. 2008;9(1):65-75. doi: 10.1038/nrn2303.
653 PubMed PMID: 18094707.
654 44. Harris DA, Tinsley RA, Walter NG. Terbium-mediated footprinting probes a catalytic
655 conformational switch in the antigenomic hepatitis delta virus ribozyme. J Mol Biol.
656 2004;341(2):389-403. doi: 10.1016/j.jmb.2004.05.074. PubMed PMID: 15276831.
657 45. Hua Y, Sahashi K, Hung G, Rigo F, Passini MA, Bennett CF, et al. Antisense correction of
658 SMN2 splicing in the CNS rescues necrosis in a type III SMA mouse model. Genes Dev.
659 2010;24(15):1634-44. doi: 10.1101/gad.1941310. PubMed PMID: 20624852; PubMed Central
660 PMCID: PMCPMC2912561.
661 46. Du L, Richter JD. Activity-dependent polyadenylation in neurons. RNA. 2005;11(9):1340-7.
662 doi: 10.1261/rna.2870505. PubMed PMID: 16043499; PubMed Central PMCID:
663 PMCPMC1370817.
664 47. Pavlopoulos E, Trifilieff P, Chevaleyre V, Fioriti L, Zairis S, Pagano A, et al. Neuralized1
665 activates CPEB3: a function for nonproteolytic ubiquitin in synaptic plasticity and memory
666 storage. Cell. 2011;147(6):1369-83. doi: 10.1016/j.cell.2011.09.056. PubMed PMID: 22153079;
667 PubMed Central PMCID: PMCPMC3442370.
668 48. Chao HW, Lai YT, Lu YL, Lin CL, Mai W, Huang YS. NMDAR signaling facilitates the IPO5-
669 mediated nuclear import of CPEB3. Nucleic Acids Res. 2012;40(17):8484-98. doi:
670 10.1093/nar/gks598. PubMed PMID: 22730302; PubMed Central PMCID: PMCPMC3458550.
671 49. Vogel-Ciernia A, Wood MA. Examining object location and object recognition memory in mice.
672 Curr Protoc Neurosci. 2014;69:8 31 1-17. doi: 10.1002/0471142301.ns0831s69. PubMed PMID:
673 25297693; PubMed Central PMCID: PMCPMC4219523.
674 50. Kandel ER. The molecular biology of memory storage: a dialogue between genes and synapses.
675 Science. 2001;294(5544):1030-8. doi: 10.1126/science.1067020. PubMed PMID: 11691980.
676 51. Frey U, Morris RGM. Synaptic tagging and long-term potentiation. Nature.
677 1997;385(6616):533-6. doi: DOI 10.1038/385533a0. PubMed PMID:
678 WOS:A1997WG23500047.
679 52. Richter JD. Translational control of synaptic plasticity. Biochem Soc T. 2010;38:1527-30. doi:
680 10.1042/Bst0381527. PubMed PMID: WOS:000285813100024.
681 53. Neugebauer KM. Nascent RNA and the Coordination of Splicing with Transcription. Csh
682 Perspect Biol. 2019;11(8). doi: ARTN a032227
683 10.1101/cshperspect.a032227. PubMed PMID: WOS:000482756900001.
684 54. Reimer KA, Mimoso CA, Adelman K, Neugebauer KM. Co-transcriptional splicing regulates 3′
685 end cleavage during mammalian erythropoiesis. Molecular Cell. 2021. doi:
686 https://doi.org/10.1016/j.molcel.2020.12.018.
687 55. Diering GH, Huganir RL. The AMPA Receptor Code of Synaptic Plasticity. Neuron.
688 2018;100(2):314-29. doi: 10.1016/j.neuron.2018.10.018. PubMed PMID: 30359599; PubMed
689 Central PMCID: PMCPMC6214363.
690 56. Si K, Kandel ER. The Role of Functional Prion-Like Proteins in the Persistence of Memory.
691 Cold Spring Harb Perspect Biol. 2016;8(4):a021774. doi: 10.1101/cshperspect.a021774.
692 PubMed PMID: 27037416; PubMed Central PMCID: PMCPMC4817803.
693 57. Seth PP, Siwkowski A, Allerson CR, Vasquez G, Lee S, Prakash TP, et al. Short antisense
694 oligonucleotides with novel 2'-4' conformationaly restricted nucleoside analogues show
695 improved potency without increased toxicity in animals. J Med Chem. 2009;52(1):10-3. doi:
696 10.1021/jm801294h. PubMed PMID: 19086780.
697 58. Wirths O. Preparation of Crude Synaptosomal Fractions from Mouse Brains and Spinal Cords.
698 Bio-Protocol. 2017;7(15). doi: ARTN e2423
699 10.21769/BioProtoc.2423. PubMed PMID: WOS:000457836100005.
700

Acknowledgments

We thank M. Malgowska , C-K. Lau, and M. A. Sta Maria for experimental assistance.

Funding:
National Institutes of Health grant R01AG051807 (MAW)
National Institutes of Health grant RF1AG057558 (MAW)
National Science Foundation 1804220 (AL)
National Science Foundation 1330606 (AL)
National Science Foundation Graduate Research Fellowship (CCC)

Author contributions:

Design of cell culture experiments: CCC, XL, TWB, AL
Design of mouse experiments: CCC, MAW, AL
In vitro ribozyme kinetics measurements: MM
Design of ASOs: MN
Cell culture experiments: CCC, LT, XL
Mouse experiments: CCC
Stereotaxic surgeries and in vivo behavior experiments: JH, CC
Data analysis: CCC
Writing—original draft: CCC, AL
Writing—review & editing: CCC, MN, XL, LT, TWB, MAW, AL

Competing interests: All other authors declare they have no competing interests.

Data and materials availability: All data are available in the main text or the supplementary materials.

732 **Figures and Tables**

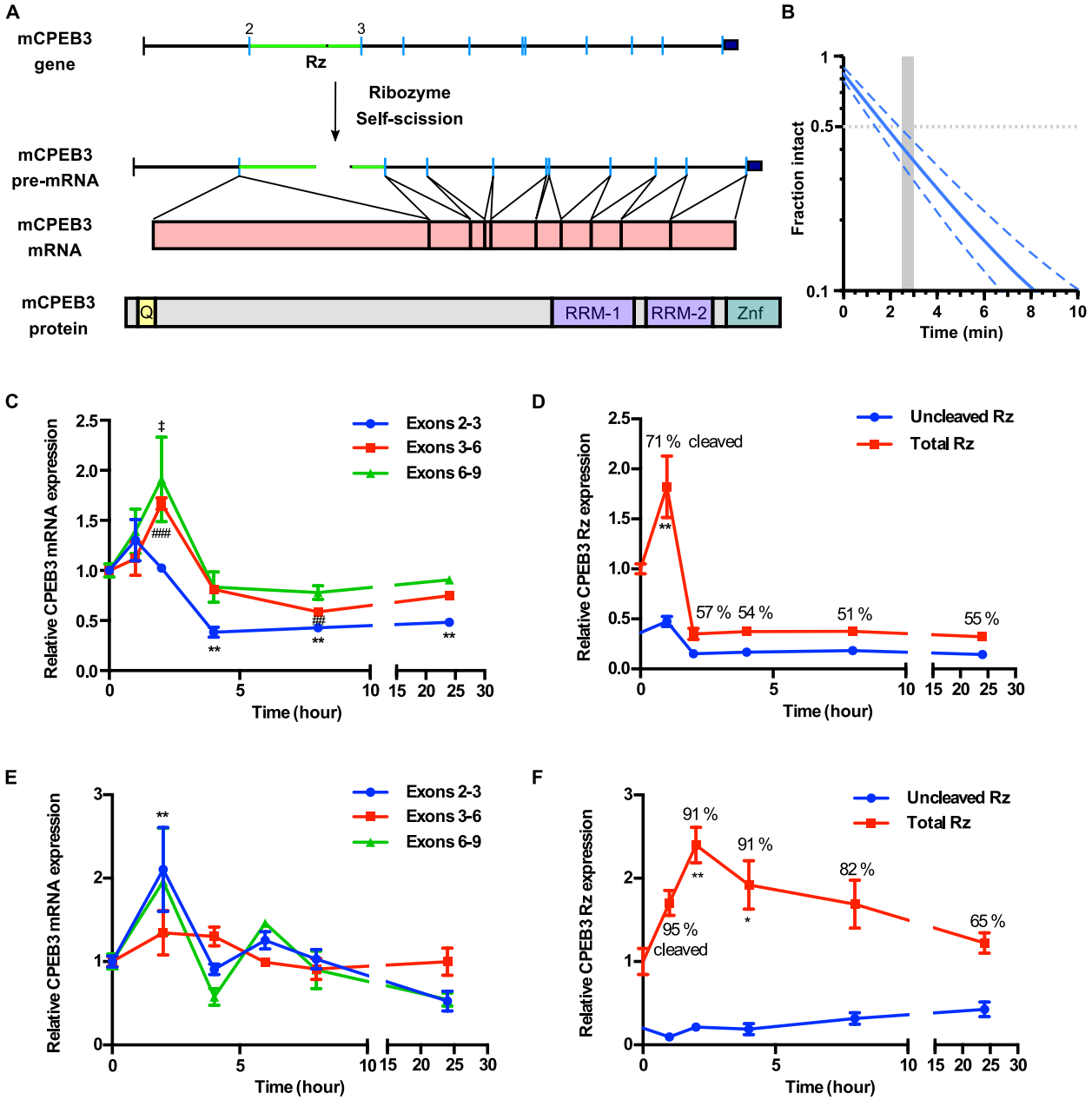

733
734 **Fig 1. CPEB3 ribozyme activity and its effect on primary cortical neurons.** (A) Schematic
735 representation of mouse *CPEB3* gene and its products. Rz denotes the ribozyme location in
736 the 2nd intron (green) between the 2nd and 3rd exons. Co-transcriptional self-scission is shown
737 by a break in the pre-mRNA 2nd intron. Fully-spliced mRNA is shown independent of the
738 ribozyme activity. (B) Co-transcriptional self-cleavage activity of a 470-nt construct,
739 incorporating the 72-nt ribozyme, which cuts the transcript 233 nts from the 5′ terminus (see
740 Table S1 for kinetic parameters of this and other constructs). Log-linear graph of self-

741 cleavage is shown with solid blue line (dashed lines show ± standard deviation). Gray dotted
742 line indicates mid-point of self-cleavage (with resulting $t_{1/2}$ of ~2 min). Gray bar indicates the
743 approximate time range for RNAPII to reach from the ribozyme to the 3rd exon, at which
744 point ~40% of the intron would remain intact. (C) KCl stimulation profile of the *CPEB3* gene
745 showing induction of spliced CPEB3 exons (one-way ANOVA with Sidak's *post hoc* tests.
746 $*P < 0.05$, $**P < 0.01$, $\#\#P < 0.01$, $\#\#\#P < 0.001$, ‡$P < 0.05$). (D) KCl stimulation profile of
747 CPEB3 ribozyme expression (uncleaved and total). Cleaved ribozyme fraction is calculated as
748 [(total ribozyme – uncleaved ribozyme)/total ribozyme] and shown as % cleaved. (E)
749 Expression of CPEB3 mRNA exons 2–3 is upregulated 2 hours after glutamate stimulation
750 (one-way ANOVA with Sidak's multiple comparisons *post hoc* test. $**P < 0.01$). (F)
751 Glutamate stimulation induces an increase in CPEB3 ribozyme levels at 2-hour time point
752 (one-way ANOVA with Sidak's multiple comparisons *post hoc* test. $*P < 0.05$, $**P < 0.01$).
753 Data are presented as mean ± SEM.

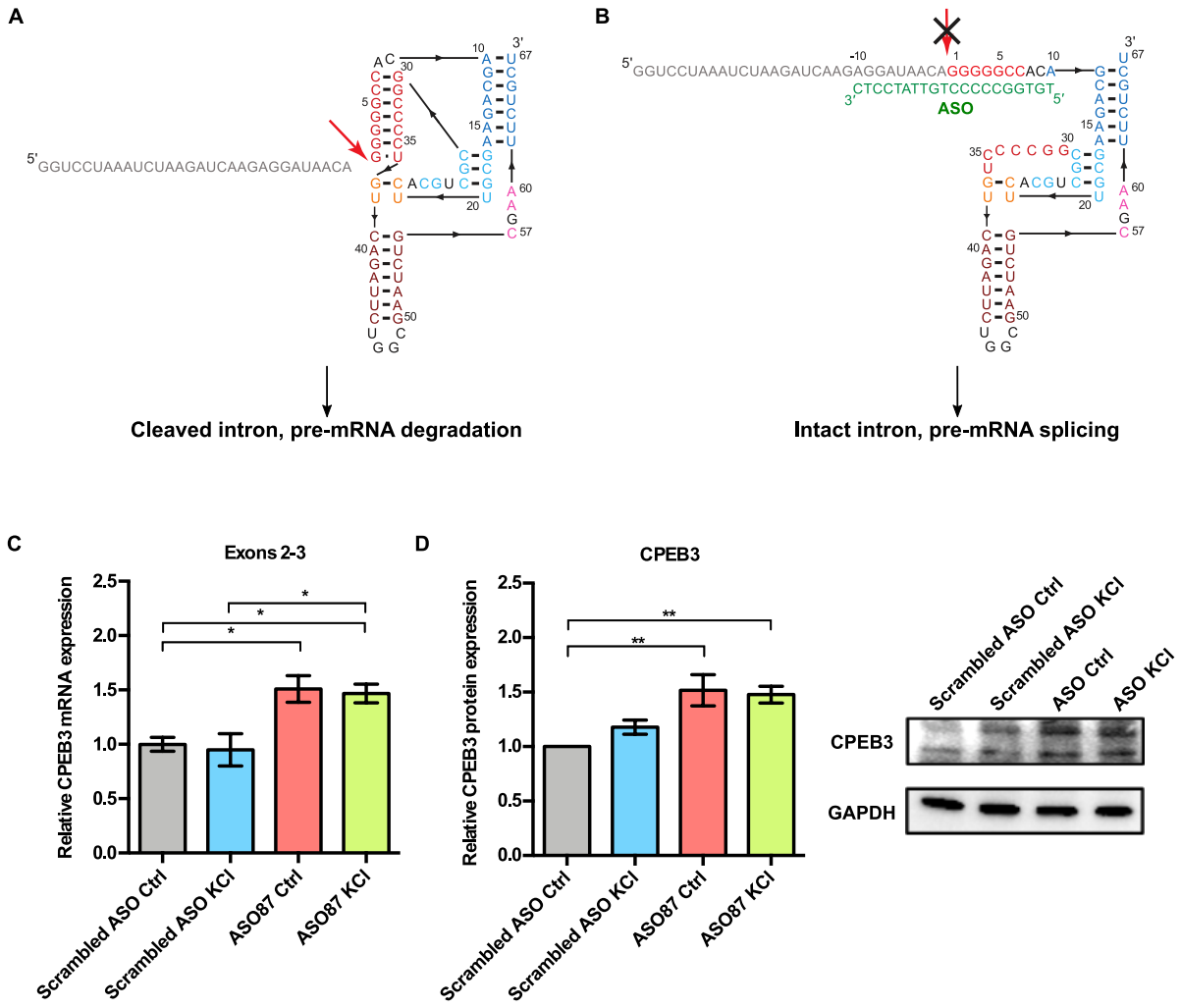

Fig 2. CPEB3 mRNA and protein are upregulated in primary neuronal cultures treated with ASO. (A) Inhibition of the CPEB3 ribozyme by an ASO targeting its cleavage site. Secondary structure of the ribozyme (colored by structural elements [10]). Sequence upstream of the ribozyme is shown in gray, and the site of self-scission is shown with the red arrow. (B) Model of the ribozyme inhibited by the antisense oligonucleotide (ASO, green letters) showing base-pairing between the ASO and 10 nts upstream and downstream of the ribozyme cleavage site. Inhibition of self-scission is indicated by crossed arrow. (C) Ribozyme inhibition by ASO in cultured cortical neurons resulted in upregulation of CPEB3 mRNA (exons 2–3; one-way ANOVA with Sidak's *post hoc* tests, $*P < 0.05$). (D) Effect of CPEB3 ribozyme ASO on CPEB3 protein expression. GAPDH is used as a loading control (one-way

766 ANOVA with Sidak's *post hoc* tests, *$P < 0.05$, **$P < 0.01$). Data are presented as mean ±

767 SEM.

768

769

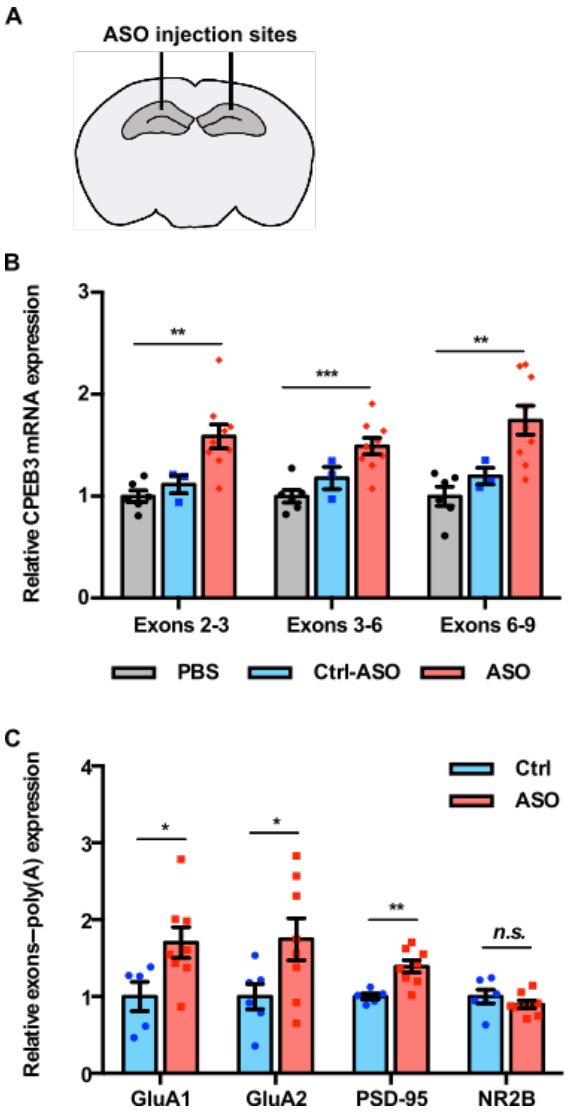

770

771 **Fig 3. CPEB3 ribozyme ASO leads to an increase of CPEB3 mRNA and polyadenylation**
772 **of PRPs in the CA1 hippocampus.** (A) Schematic representation of stereotaxic procedure.
773 ASO, scrambled ASO, or vehicle was bilaterally infused to the mouse CA1 hippocampus. (B)
774 CPEB3 mRNA expression is upregulated in the CPEB3 ribozyme ASO treatment group
775 compared to controls (one-way ANOVA with Sidak's *post hoc* tests. $^{**}P < 0.01$, $^{***}P <$
776 0.001). (C) Inhibition of CPEB3 ribozyme results in increased polyadenylation of plasticity-
777 related genes (unpaired *t* test, $^{*}P < 0.05$, $^{**}P < 0.01$, *n.s.* not significant). Data are presented
778 as mean ± SEM.

779

780

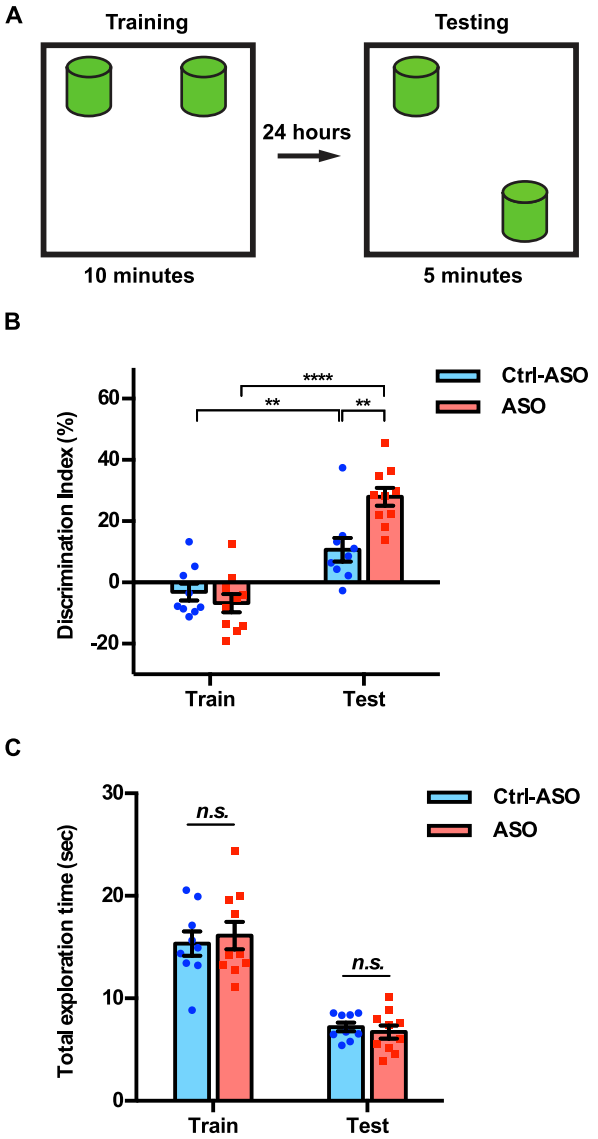

781

782 **Fig 4. Inhibition of CPEB3 ribozyme enhances long-term OLM.** (A) Experimental
783 procedure testing long-term memory. (B) Mice infused with CPEB3 ribozyme ASO show
784 significant discrimination index in OLM testing (two-way ANOVA with Sidak's *post hoc*
785 tests, $*P < 0.05$, $**P < 0.01$, $****P < 0.0001$). (C) CPEB3 ribozyme ASO and control mice
786 display similar total exploration time (one-way ANOVA with Sidak's *post hoc* tests, *n.s.* not
787 significant). Data are presented as mean ± SEM.

788

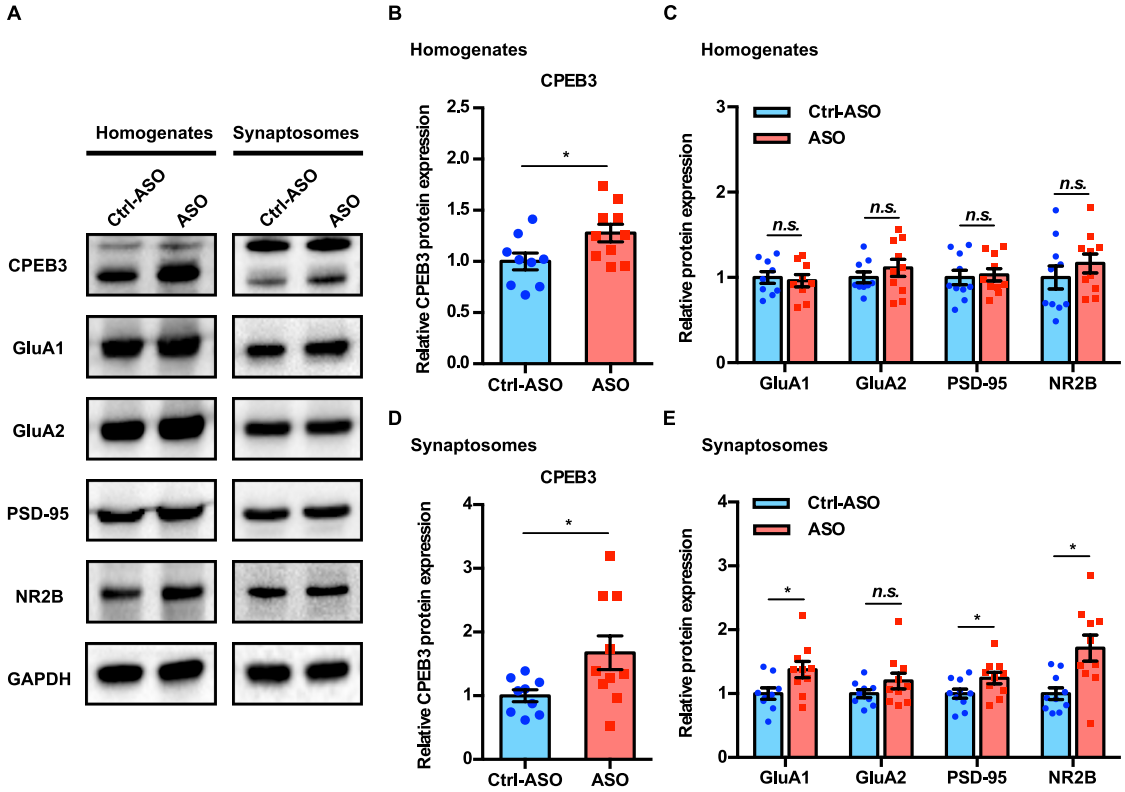

Fig 5. Inhibition of CPEB3 ribozyme leads to upregulation of CPEB3 and PRPs protein expression after OLM. (A) Representative images of immunoblotting analysis. GAPDH is used as a loading control. Quantification of CPEB3 (B) and PRPs (C) in tissue homogenates shows increased CPEB3, but not PRPs, protein expression (unpaired *t* test, $*P < 0.05$, *n.s.* not significant). (D) In synaptosomes, the protein expression of both CPEB3 (D) and PRPs (E) is increased (unpaired *t* test, $*P < 0.05$, *n.s.* not significant). Data are presented as mean ± SEM.

Supplementary Materials for

The CPEB3 ribozyme modulates hippocampal-dependent memory

Claire C. Chen, Joseph Han, Carlene A. Chinn, Xiang Li, Mehran Nikan, Marie Myszka, Liqi Tong, Timothy W. Bredy, Marcelo A. Wood*, Andrej Lupták*

*Corresponding author. Email: aluptak@uci.edu
mwood@uci.edu

This PDF file includes:

Figs S1 to S5
Tables S1 to S4

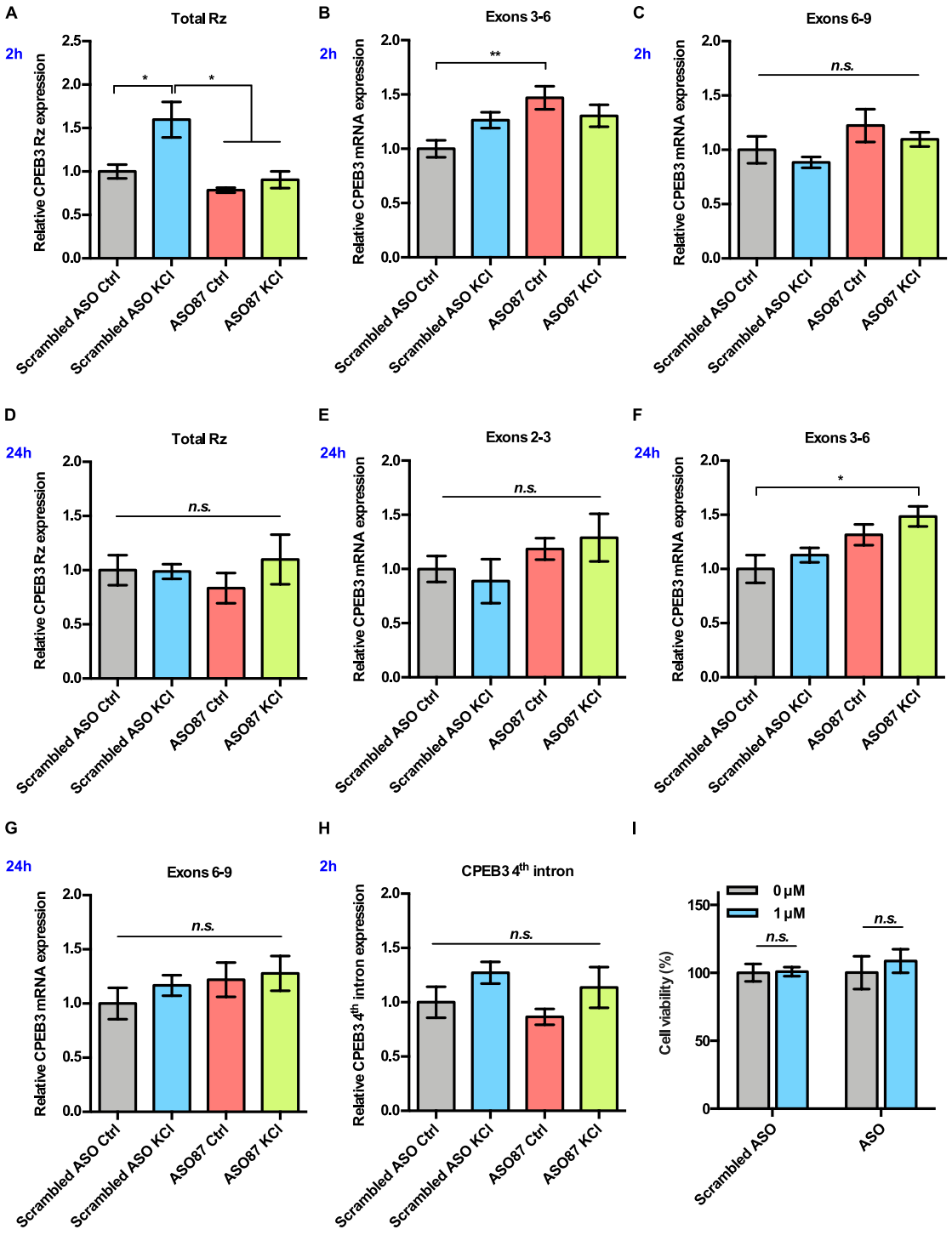

S1 Fig. Effect of CPEB3 ribozyme ASO on CPEB3 expression in embryonic cortical neurons. (A) CPEB3 ribozyme levels increase together with levels of the surrounding exons 2 hours post stimulation in experiments with control ASO. Ribozyme levels are significantly

837 lower in ribozyme ASO experiments, suggesting blocking of the RT-PCR reaction by the
838 ASO. (B) and (C) Inhibition of CPEB3 ribozyme by ASO resulted in upregulation of CPEB3
839 mRNA basal levels for exons 3–6 (B) at 2-hour time point. Levels of exons 6–9 did not
840 increase significantly (C) (one-way ANOVA with Sidak's *post hoc* tests, $^{**}P < 0.01$, *n.s.* not
841 significant). (D) No statistically significant difference in CPEB3 ribozyme expression was
842 observed after 24 hours post KCl induction (one-way ANOVA with Sidak's *post hoc* tests,
843 *n.s.* not significant), suggesting that all intronic RNA levels reached basal levels. (E) – (G)
844 CPEB3 mRNA expression largely returned to the basal level 24 hours post stimulation,
845 although levels of spliced exons 3–6 remained elevated (E: exons 2–3, F: exons 3–6, G: exons
846 6–9, one-way ANOVA with Sidak's *post hoc* tests, $^{*}P < 0.05$, *n.s.* not significant). (H) qRT-
847 PCR analysis of CPEB3 4th intron expression reveals that the ribozyme ASO does not affect
848 its levels, suggesting that it is specific for the ribozyme (one-way ANOVA with Sidak's *post*
849 *hoc* tests, *n.s.* not significant). (I) Effect of ASOs treatment on cell viability. XTT assay was
850 performed after 18 hours incubation of ASOs. Relative cell viability was normalized to the
851 vehicle control (unpaired *t* test, *n.s.* not significant). Data are presented as mean ± SEM.

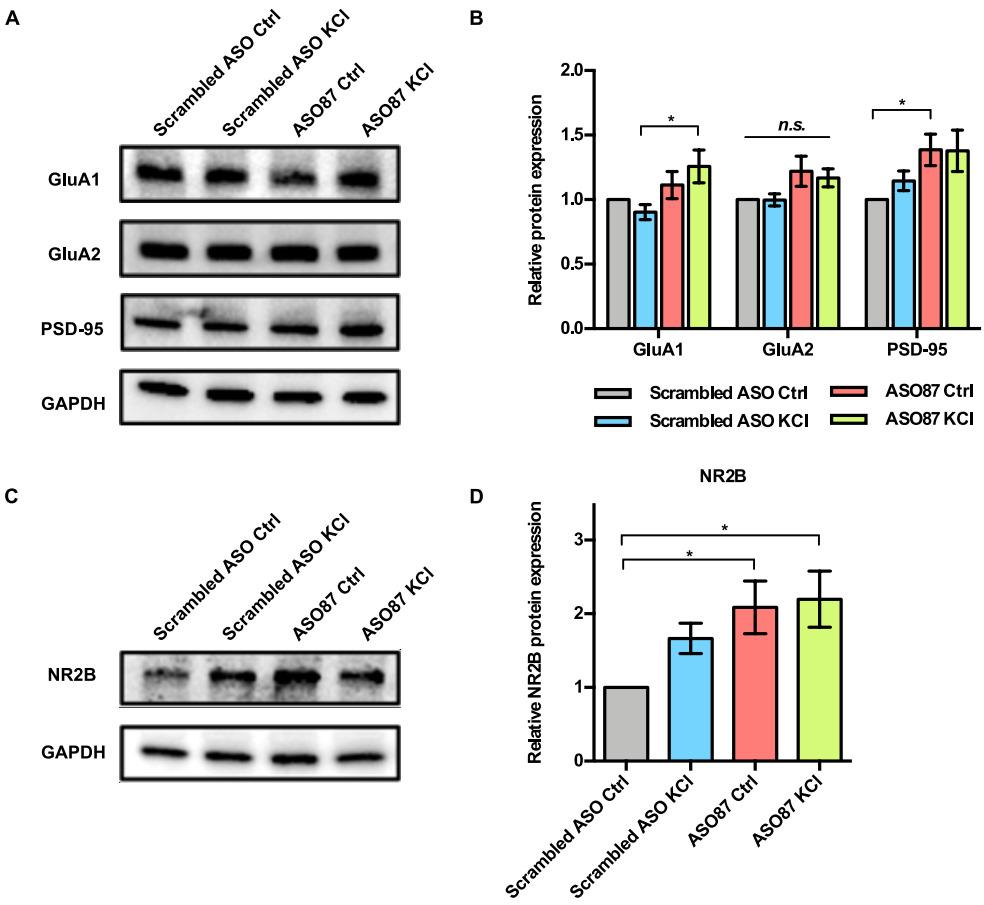

852

853 **S2 Fig. Effect of CPEB3 ribozyme ASO on protein expression in embryonic cortical**
854 **neurons.** Primary neuronal cultures were pretreated with ASO or scrambled ASO, followed
855 by KCl stimulation. Cells were harvested 8 hours after KCl induction. PRPs protein
856 expression levels were determined by immunoblotting. (A) Representative immunoblotting
857 image of GluA1, GluA2, and PSD-95 protein expression. GAPDH is used as a loading
858 control. (B) Quantification of PRPs protein expression. GluA1 expression is upregulated in
859 the presence of ASO combined with neuronal stimulation. Treatment with ASO leads to an
860 increase of PSD-95 protein level in primary cortical neurons (one-way ANOVA with Sidak's
861 *post hoc* tests. $*P < 0.05$, *n.s.* not significant. (C) Representative images of immunoblotting
862 analysis showing NR2B protein expression. GAPDH is used as a loading control. (D)
863 Quantification of NR2B protein expression. ASO treatment induces an increase in NR2B

expression (one-way ANOVA with Sidak's *post hoc* tests. $*P < 0.05$). Data are presented as mean ± SEM. The analysis revealed that the steady-state levels of GluA1 are elevated when the CPEB3 ribozyme is inhibited, but these levels do not increase further upon KCl stimulation of the cultured cortical neurons.

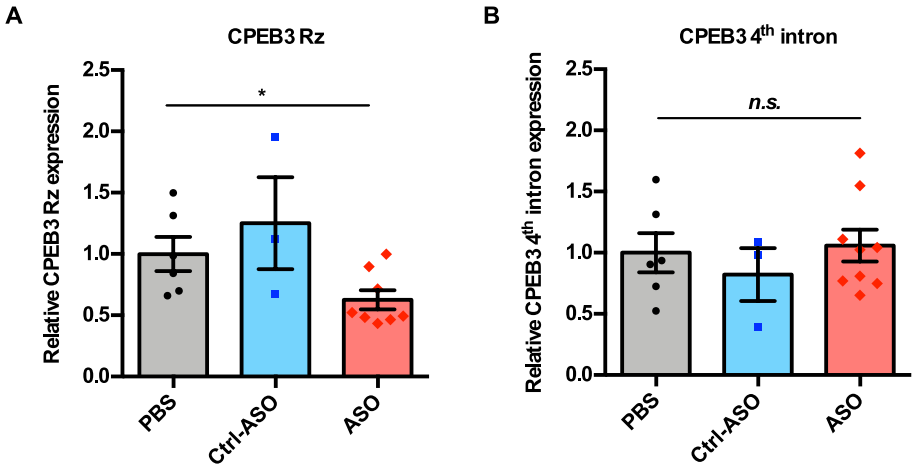

S3 Fig. Inhibition of CPEB3 ribozyme by ASO *in vivo*. (A) Validation of CPEB3 ribozyme knockdown *in vivo*. Administration of CPEB3 ribozyme ASO to the mouse CA1 hippocampus leads to a decrease in CPEB3 ribozyme levels (one-way ANOVA with Sidak's *post hoc* tests $*P < 0.05$). (B) The ribozyme ASO has high specificity for its cleavage site (in the 3rd intron) *in vivo*. qRT-PCR analysis of the 4th intron of *CPEB3* gene demonstrates no significant difference between controls and ASO groups (one-way ANOVA with Sidak's *post hoc* test, *n.s.* not significant). Data are presented as mean ± SEM.

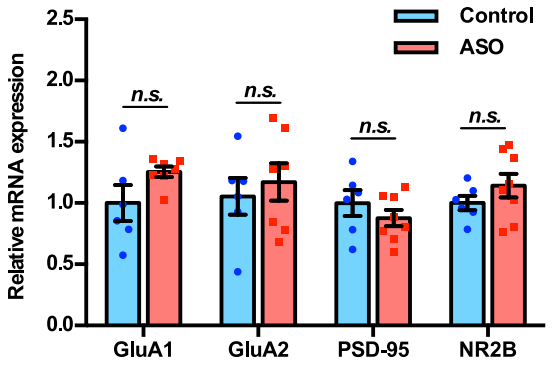

879
880 **S4 Fig. Inhibition of CPEB3 ribozyme does not affect transcription of other plasticity-**
881 **related genes**. qRT-PCR analysis of mature GluA1, GluA2, PSD-95, and NR2B mRNAs. No
882 significant difference between ASO and control was observed for splice junctions within the
883 mRNAs, showing that modulation of the CPEB3 ribozyme does not affect transcription or
884 splicing of these mRNAs (unpaired *t* test, *n.s.* not significant). Data are presented as mean ±
885 SEM.

886

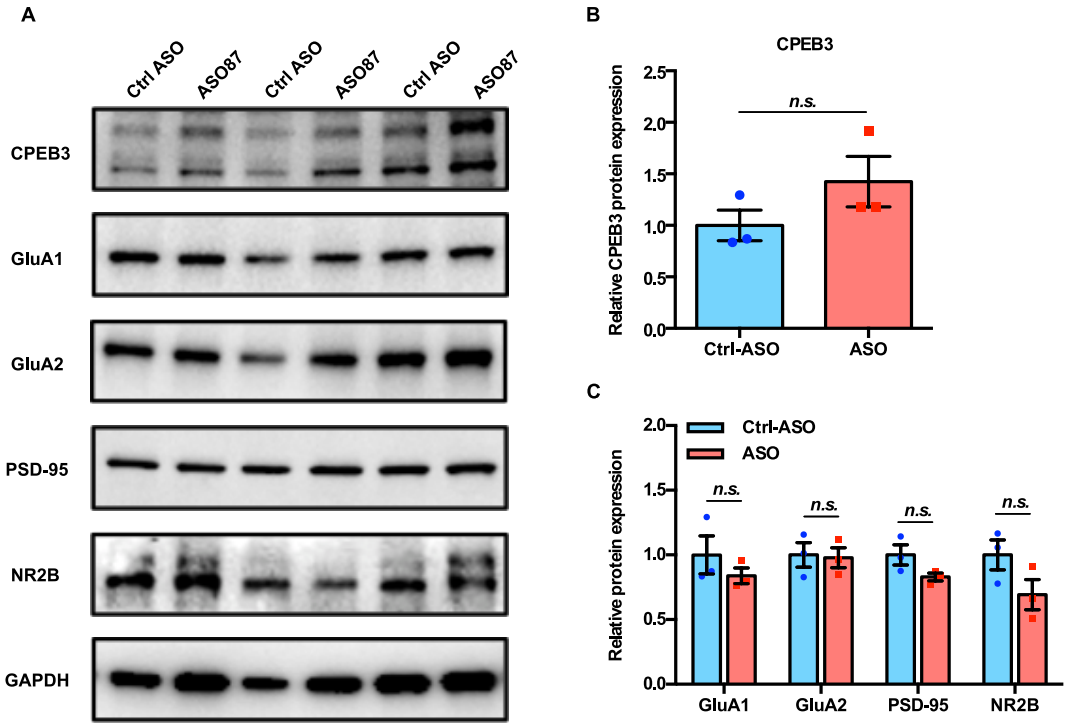

887

888 **S5 Fig. Effect of CPEB3 ribozyme on overall protein expression in the dorsal**
889 **hippocampus.** (A) Representative images of immunoblotting analysis. GAPDH is used as a
890 loading control. (B) Quantification of CPEB3 protein expression (unpaired *t* test, *n.s.* not
891 significant). (C) Quantification of PRPs protein expression (unpaired *t* test, *n.s.* not
892 significant). Data are presented as mean ± SEM.

893

894 **S1 Table. Kinetic parameters of murine CPEB3 ribozyme constructs[2]**

895

Construct[1]	A	k_1	B	k_2	C
-10/72	0.72 ± 0.09	0.39 ± 0.09			0.082 ± 0.026
-49/72/165	0.88 ± 0.02	0.42 ± 0.04	0.013 ± 0.015	0.11 ± 0.03	0.04 ± 0.02
-233/72/165	0.78 ± 0.04	0.31 ± 0.04	0.035 ± 0.006	0.17 ± 0.02	0.029 ± 0.005

896

897 [1] Construct size is defined as the length of sequence upstream of the ribozyme cleavage
898 site/CPEB3 ribozyme (72 nts)/downstream sequence.

899 [2] Co-transcriptional self-scission was modeled by a bi-exponential decay model with a residual.
900 A and B represent fractions of the population cleaving with fast (k_1) and slow (k_2) rate constants,
901 respectively. The residual (C) is interpreted as a fraction of the population that does not self-
902 cleave. Errors represent SEM of at least three experiments. For the smallest ribozyme construct
903 (-10/72), a monoexponential decay function was sufficient to model the data.

904

905 **S2 Table. Primers used in qPCR**

Target		Sequence
CPEB3 exons 2–3	Forward	CGATAATGGTAACAATCTGTTGCC
	Reverse	CCTTATCATATCCATTAAGGAGTTCTCC
CPEB3 exons 3–6	Forward	GACCGGAGTAGGCCCTATGA
	Reverse	CCAGACGATAAGGCCTGATCA
CPEB3 exons 6–9	Forward	ACTCTAGAAAGGTGTTTGTTGGAGG
	Reverse	TCGAAGGGGTCGTGGAACT
CPEB3 ribozyme cleaved	Forward	GTTCACGTCGCGGCC
	Reverse	GTGATATAGTGTGTTCTTCAGTGACTCCT
CPEB3 ribozyme uncleaved	Forward	CCAAGCAGCAGCACAGGTC
	Reverse	GTGATATAGTGTGTTCTTCAGTGACTCCT
CPEB3 4th intron	Forward	CACTCTAGCCTAACTGGTGAGCTC
	Reverse	AGTCATTCCAACAGAAATGAAGTACC
GluA1	Forward	GTCCGCCCTGAGAAATCCAG
	Reverse	CTCGCCCTTGTCGTACCAC
GluA2	Forward	TGGTACGACAAAGGAGAGTGC
	Reverse	ACCAGCATTGCCAAACCAAG
PSD-95	Forward	TGAGATCAGTCATAGCAGCTACT
	Reverse	CTTCCTCCCCTAGCAGGTCC
NR2B	Forward	GCCATGAACGAGACTGACCC
	Reverse	GCTTCCTGGTCCGTGTCATC
GAPDH	Forward	TGACCACAGTCCATGCCATC
	Reverse	GACGGACACATTGGGGGTAG

906

907

908 **S3 Table. Antibodies used in immunoblotting analysis**

Antigen	Species	Company	Catalog #	Dilution
CPEB3	Rabbit	Abcam	ab18833	1:1,000
GluA1	Mouse	UC Davis/NIH NeuroMab Facility	75-327	1:1,000
GluA2	Rabbit	Proteintech	11994-1-AP	1:2,000
PSD-95	Rabbit	Proteintech	20665-1-AP	1:2,000
NR2B	Rabbit	Proteintech	21920-1-AP	1:2,000
GAPDH	Mouse	Proteintech	60004-1-Ig	1:10,000
Anti-rabbit HRP	Donkey	Thermo Fisher Scientific	A16023	1:10,000
Anti-mouse HRP	Goat	R&D system	HAF007	1:1,000

909 **S4 Table. Primers used in 3′ RACE**

Target	Sequence
3′ RACE adaptor	CCAGTGAGCAGAGTGACGAGGACTCGAGCTCAAGCTTTTTTTTTTTTTTTT TTTT
3′ RACE outer primer	CCAGTGAGCAGAGTGACG
3′ RACE inner primer	GAGGACTCGAGCTCAAGC
GluA1	GGTCCGCCCTGAGAGGTCCC
GluA1 nested	CCTGAGCAATGTGGCAGGCGT
GluA2	GCTACGGCATCGCCACACCT
GluA2 nested	ATCCTTGTCGGGGGCCTTGGT
PSD-95	GGCCACGAAGCTGGAGCAGG
PSD-95 nested	GGCCTGGACTCACCCTGCCT
NR2B	GAGACGAAGGCTGCAAGCTGGT
NR2B nested	CGCCAGGTGGACCTTGCTATCC

910
911
912